



Developing plating baths for the production of reflective Ni–Cu films

P. Calleja^a, J. Esteve^b, P. Cojocar^c, L. Magagnin^c, E. Vallés^a, E. Gómez^{a,*}

^a *Electrodep. Departament de Química Física, Universitat de Barcelona, 08028 Barcelona, Spain*

^b *Departament de Física Aplicada i Òptica, Universitat de Barcelona, 08028 Barcelona, Spain*

^c *Dipartimento di Chimica, Materiali e Ingegneria Chimica "Giulio Natta", Politecnico di Milano, 20131 Milano, Italy*

ARTICLE INFO

Article history:

Received 27 July 2011

Received in revised form

12 December 2011

Accepted 12 December 2011

Available online 19 December 2011

Keywords:

Electrodeposition

Ni–Cu alloy

Gloss

Reflectivity

ABSTRACT

Electrolytic baths have been developed to obtain bright nickel–rich nickel–copper micrometric films with good mechanical properties and high reflectivity, valid as components of optical mirrors. As metal source, the developed baths contain nickel (II) sulfamate and copper (II) acetate. Citrate was used as buffer and complexing agent to favour the simultaneous electrodeposition of copper and nickel. The influence of citrate concentration, solution pH, [Ni(II)]/[Cu(II)] ratio and applied potential on the composition was studied. In order to achieve constant composition throughout the deposit thickness, potentiostatic technique was selected. The optimization process was followed according to a simple factorial design. By adjusting the conditions, compact, uniform and fine grained nickel–copper (Ni–Cu) electrodeposits with high Ni percentages and low roughness were obtained. The deposits show mechanical properties suitable for electroforming. The optical properties (reflectivity and gloss) of the Ni–Cu films make them adequate to be elements of optical mirrors.

© 2011 Elsevier Ltd. All rights reserved.

1. Introduction

Aerospace industry requires lightweight mirror shells as mirror modules of the telescopes [1]. Various technologies have been developed for the production of these such as galvanoplastic replication or direct polishing [2]. Different studies demonstrated that electroforming allows mirror shell production with large optical surface area, enabling the production of low cost, isotropic, precision optical shell-like reflectors highlighting excellent performances. In principle, any reflector thickness can be electroformed with the desired curvature and surface characteristics close to the optical quality of the mandrel. Electroforming offers the ability to precisely replicate in a hard, wear-resistant metal a pattern by electrodeposition in a suitable electrolyte. Another benefit of this technology is the ability to replicate sequentially, thus producing mirrors from only one master. Replicated nickel optics have been used extensively in X-ray astronomy. In the electroformed replication (ER) fabrication process, nickel mirror shells are electroformed onto a figured and superpolished mandrel. Afterwards, mirror shells are released from the mandrel using differential thermal contraction [3]. This technique involves forming an extremely lightweight mirror by electroplating nickel and nickel-based alloys onto a highly polished precision mandrel [4]. For such an optical electroform to be usable, it does have to meet

several requirements: surface finish, dimensional tolerances and flatness or radius of curvature have to closely match the original. This can only be accomplished if internal stresses in the electroformed layer are kept to a minimum. These can be explained as the tendency of the deposited layer to either contract (tensile stress) or expand (compressive stress) relative to the substrate upon separation from it. This is determined by a number of factors, such as deposition rate, bath chemistry, additives, agitation, etc. To ensure compositional uniformity of the finished product, solution conditions must be controlled within a narrow range, the parameters being regularly checked and adjusted. The electrodeposition of the Ni–Cu system has attracted much attention and it has been widely treated due to the high versatility of applications of this alloy. These applications derive from their electrocatalytic properties [5–7], magnetic or magnetoresistive properties [8–13], their anticorrosion properties [14], the recent exploited thermoelectric properties [15–17], as well as their mechanical strength [18,19] and reasonably good wear resistance [20–22]. Depending on the final application, different electrolytic baths has been proposed, which led to variable percentages of the metals in the alloy [18,23–25].

The main interest of this contribution is the study of the process of development of nickel–copper baths able to prepare nickel–copper (Ni–Cu) alloys which could be used in optical mirror production. The combination of good corrosion resistance and interesting mechanical properties makes Ni–Cu alloy suitable. Low copper proportions are desirable to improve nickel mechanical properties while maintaining high film gloss and reflectivity.

* Corresponding author. Tel.: +34 934021234; fax: +34 934021231.

E-mail address: e.gomez@ub.edu (E. Gómez).

In order to facilitate codeposition, citrate was selected as a common complexing agent for Ni–Cu baths [26–33], since it not only has a low toxicity but does also act as a brightening [23], levelling [34] and buffering agent [35], thus eliminating the need for other bath additives. Despite the numerous studies performed regarding obtaining nickel–copper alloy, are few ones devoted to prepare rich nickel deposits, and their results make difficult to draw conclusions in acidic media. Moreover, as some citrate nickel–copper baths proposed in the literature show instability [26,27] related in some cases to specific complex formation [36,37], a step by step process was considered to develop the basic bath formulation. Firstly, for the selected salts, single-metal deposition behaviour was studied at different citrate concentrations and solution pH. Our objective was producing, from solutions with low $[\text{Cu(II)}]/[\text{Ni(II)}]$ ratio, Ni–Cu films with no less than 75 wt.% Ni, having in mind the bath stability. The deposit quality and compositional variation obtained from each bath was evaluated prior to selecting conditions. This optimization process was followed according to a simple factorial design [38], in which we found the significant effects that exert the main interaction in the general behaviour in the screening step. This was followed by an optimization process in which the conditions leading to the best response were defined.

2. Experimental

The electrochemical measurements were performed in a conventional three-electrode cell using an Autolab with PGSTAT30 equipment and GPES software. Chemicals used were $\text{Ni}(\text{H}_2\text{NSO}_3)_2 \cdot 4\text{H}_2\text{O}$ (nickel sulfamate), $(\text{CH}_3\text{COO})_2\text{Cu} \cdot \text{H}_2\text{O}$ (copper acetate) and $\text{Na}_3\text{C}_6\text{H}_5\text{O}_7 \cdot 2\text{H}_2\text{O}$ (sodium citrate), all of analytical grade. Sulfamate, citrate and acetate were selected as being less aggressive with the environment. All solutions were freshly prepared with water first doubly distilled and then treated with a Millipore Milli Q system. Before and during the experiments, solutions were de-aerated with argon. The temperature was maintained at 25 °C.

Working electrodes were vitreous carbon (Metrohm) used for the basic electrochemical study and inox steel to grow the films. The vitreous carbon electrode was polished to a mirror finish with alumina of different grades (3.75 and 1.87 μm) and ultrasonically cleaned for 2 min in water before each experiment. Prior to the electrodeposition inox steel (stainless steel AISI 316 with maximum percentages of C, Mn, Cr, Ni and Mo of 0.05, 2, 17, 12 and 2.5 wt.% respectively) was polished with grit paper (FEPA p \neq 4000) and washed with abundant water. The reference electrode was an $\text{Ag}/\text{AgCl}/1 \text{ mol dm}^{-3} \text{ NaCl}$ electrode mounted in a Luggin capillary containing 0.25 mol dm^{-3} sodium sulfamate solution. All potentials were referred to this electrode. The counter electrode was a platinum spiral in the basic study on vitreous carbon or a Ni sheet during the preparation of deposits.

Deposit morphology was examined with a Hitachi 2300 scanning electron microscopy and the resolution of the grain with a Hitachi H-4100 FE field emission (FE-SEM). Elemental composition was determined with an X-ray analyzer incorporated in Leica Stereoscan S-360 equipment. The structure was resolved with X-ray powder diffraction (XRD), using a conventional Bragg–Brentano diffractometer Siemens D-500. The Cu $K\alpha$ radiation ($\lambda = 1.5418 \text{ \AA}$) was selected using a diffracted beam curved graphite monochromator. The X-ray powder diffraction diagrams were measured in the 5–100° 2θ range with a step range of 0.016° and a measuring time of 100 s per step.

Ni–Cu coatings were characterised in terms of micromechanical properties. Vickers microhardness (HV) data were obtained from penetration depth-load curves by means of a FISCHERSCOPE® H100 microhardness measurement system. Measurements

were as follows: 250 mN peak load, 10 s loading/unloading time and 5 s holding time at peak load. The reported values are the average of 5 measurements taken on three different samples prepared in the same conditions from the same bath. To analyse the roughness of the deposits an interferometric surface analysis microscope Plu Neox 3D optical Profiler of Sensofar was used.

Electrical resistivity of the different alloys has been measured after the thin foils have been detached from their inox substrate. The foils have been cut to an approximate square shape and the electrical measurements have been done according to Van der Paw [39] with four electrical contacts located at the four corners of the square sample. DC current (100 μA) was injected between two adjacent contacts and DC voltage was measured at the two opposite contacts. This procedure has the benefit of not requiring cutting a precise shape stripe from the small foil piece and furthermore it does not require perfect electrical contacts: pressure springs are enough (measurement results have been contrasted with measurements on strip-shaped pieces with two copper wire electrical contacts welded at the edges). Four contacting schemes are possible by cycling the square corners. For each contacting scheme two measurements are done by reversing the current polarity and two more measurements by reversing the voltage contacts. In total this meant 16 voltage measurement values that were added together to obtain sample's resistivity. It is necessary, in addition, to precisely know the foil thickness. This was measured by two methods: metallographic embedment of the foil and measurement of the foil edge thickness from its SEM micrograph. And also by direct mechanical contact: by using a precision Mitutoyo micrometer fitted with a spherical anvil.

Gloss measurements were conducted with a BYK-Gardner micro-gloss meter with an extended beam white light, and a 60° measurement angle. Sample surface should be carefully cleaned before measurement, by wiping it with an optical cleaning cloth and ethanol, in order to obtain consistent results. The calibration was performed automatically by means of a highly polished black standard integrated in the glossmeter. Multiple measurements with each coating were made in order to evaluate data statistically.

Spectral reflectivity measurements were conducted with the help of an OceanOptics fiber-optic spectrophotometer USB4000 with a reflection probe designed for quasi-perpendicular reflectance (3° measurement angle). The collected reflectivity spectra extend in the visible range (400–750 nm) and were normalised against two reference standards: a high reflectivity (96%) aluminum standard mirror and a flat spectrum magnesium oxide standard plate.

3. Results and discussion

3.1. Ni and Cu deposition behaviour

Ni and Cu deposition was analysed as a function of the citrate concentration and the solution pH. Attending to the wide difference between the standard potentials of nickel and copper, citrate was used as complexing agent to decrease the difference between the deposition potentials of both metals; the influence of the citrate concentration was analysed between 0 and 0.25 M. The pH was varied between 3 and 6 because more acidic media could favour hydrogen codeposition and higher ones lead to instabilities. Solutions with analytical concentration of 0.025 M for $[\text{Cu(II)}]$ and 0.5 M for $[\text{Ni(II)}]$ were tested for this study.

The percentage of each species in solution was calculated using the MEDUSA–Chemical Diagrams (2.0) and HYDRA–Hydrochemical Database (2.0) Softwares [40,41]. From the selected concentrations

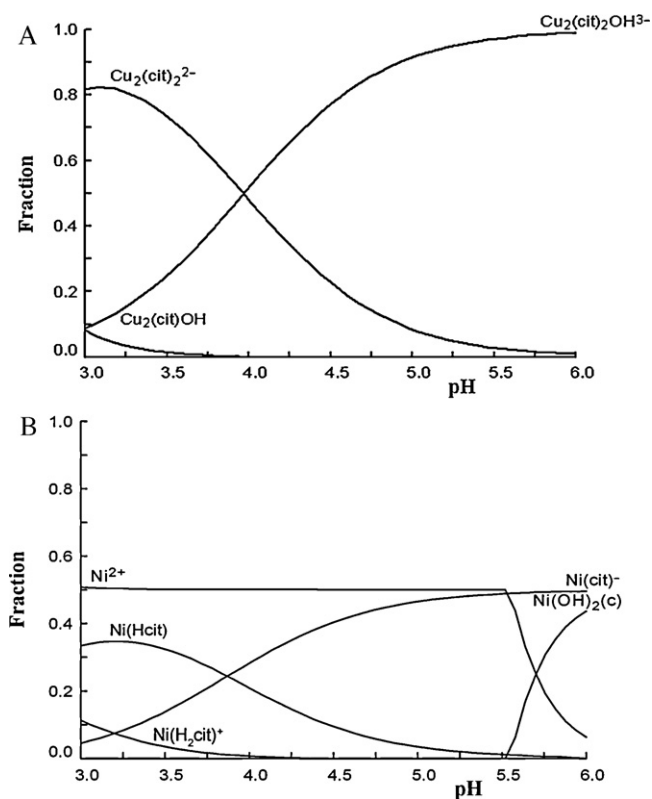


Fig. 1. Diagrams of M(II)-citrate complexes present in solution for 0.25 M $\text{Na}_3\text{C}_6\text{H}_5\text{O}_7$ and M(II): (A) 0.025 M Cu(II) and (B) 0.5 M Ni(II).

of sodium citrate and copper acetate (or nickel sulfamate), the ionic strength, the bath temperature and the stability constants of the metallic cations with the citrate species were considered. From the Hydra Database, the proportion of the different metal-citrate complexes as a function of the pH of solution was estimated. Fig. 1 shows the predominant species of copper (II) (Fig. 1A) and nickel (II) (Fig. 1B) complexes in citrate solution as a function of the solution pH.

Electrochemical behaviour of the separate metallic cations was followed at all conditions by means of voltammetric experiments. Fig. 2A shows the effect of successive citrate additions to a copper solution. On increasing citrate content, reduction process onset was delayed to more negative potentials. For a fixed analytical citrate concentration, reduction current appeared at more negative potentials as pH increased (Fig. 2B). In both cases, the shift of the onset of the deposition process to negative potentials was a consequence of a higher copper (II) complexation.

Citrate also complexes with nickel, but in lower proportion than with copper. Then, at fixed pH, moderate shift of the nickel deposition onset by increasing citrate concentration was observed (Fig. 2C).

In view of this, citrate confirms as a good election indeed. High citrate concentrations and pH values in the selected 3–6 range, favoured the approximation of the Cu deposition to the Ni(II) reduction. Nevertheless, the 0.5 M nickel sulfamate solution containing 0.25 M citrate did show instability, especially at pH 6, since precipitates were observed one week after preparation. Similar occurs at pH 6 when copper acetate is present. Reason because it was considered to reduce the $[\text{Ni}(\text{II})]$, solutions containing 0.25 M of nickel sulfamate were selected to analyse the Ni–Cu deposition in the screening step, in order to avoid the formation of precipitates.

3.2. Ni–Cu deposition

3.2.1. Screening step

In the screening step, different parameters have been fixed: a $[\text{Ni}(\text{II})]/[\text{Cu}(\text{II})]$ ratio of 20, as copper is nobler than nickel, citrate concentration of 0.25 M and a temperature of 25 °C. Solution pH (between 3 and 6) and applied potential were considered as variable parameters. For each one of the solutions analysed, the applied potential range was selected from the corresponding voltammetric study.

For all solutions studied, negative voltammetric scan shows a first peak due to copper (II) reduction (Fig. 3A, curve a); following the scan, an important current increase appeared when simultaneous nickel codeposition began (Fig. 3A, curve b), followed by hydrogen evolution (Fig. 3A, curve c). In the positive scan, independently of the cathodic limit, an oxidation peak centred on 50 mV appeared. A second oxidation peak, at 175 mV is observed only at intermediate deposition potentials (Fig. 3A, curve b), when the scan was reversed near the onset of nickel deposition. When the scan was reversed before Ni codeposition (curve a), the oxidation peak corresponds only to Cu oxidation. When Ni begins to electrodeposit (curve b), the oxidation scan reflects the Cu oxidation peak of the initial deposited Cu and the peak corresponding to the oxidation of the Cu present in the alloy or directly to Cu-rich alloy, at more positive potentials due to the presence of Ni. When the scan is reversed at more negative potentials (curve c) Ni content in the alloy must increase and moreover, significant hydrogen evolution occurs. The formation of hydroxides, due to the increase of the local pH, hinders the oxidation and the oxidation peak recorded corresponds to the copper not covered/not affected by the hydroxides. The Ni alloy oxidation is not observed in a similar way that occurs in pure electrodeposited nickel.

The voltammetric curves were sensitive to the solution stirring: an increasing stirring causes a continuous increase in the reduction charge (Fig. 3B), as occurs in other baths [37]. Only the Cu oxidation peak is observed as expected for a cathodic limit of -1.4V ; the observation of nickel or alloy oxidation is not expected in these conditions in according to the results shown in Fig. 3A. The charge involved in the Cu oxidation peak increases with the stirring rate because more Cu is deposited.

For each solution, the potential range at which Ni and Cu codeposit was selected. Samples of -25mC were prepared using potentiostatic technique in order to evaluate composition. Galvanostatic technique was not used since no constant potential was attained, which could lead to a variation in the composition–thickness profile. The solutions were gently stirred (300 rpm) during the deposition in order to prevent copper (II) depletion, the less concentrated electroactive species, in electrode environment during the deposition process. Greater stirring rate was discarded to avoid excessive copper incorporation into the deposits, because the increase in the agitation led to an increase in the copper content [42]. Stirring is also useful to prevent the possible both local pH variation caused by the possible hydrogen coevolution, and the subsequent precipitation of hydroxides. j - t profiles of deposits preparation under stirring conditions showed quasi-stabilization of the current at each potential applied (Fig. 4).

From all solutions studied, obtained deposits were metallic grey in colour at nickel percentages high enough. Nickel-rich coatings prepared were homogeneous, compact, smooth and fine-grained as the manner that grains were hardly observed by SEM, Fig. 5 corresponds to a representative image of this kind of deposits. Table 1 shows the compositional analysis of some deposits prepared. Nickel content increased significantly as the applied potential decreased, but levelling off at the more negative applied potentials. Deposits obtained at fixed electrodeposition conditions but at variable deposition times showed the same composition. This proves that the

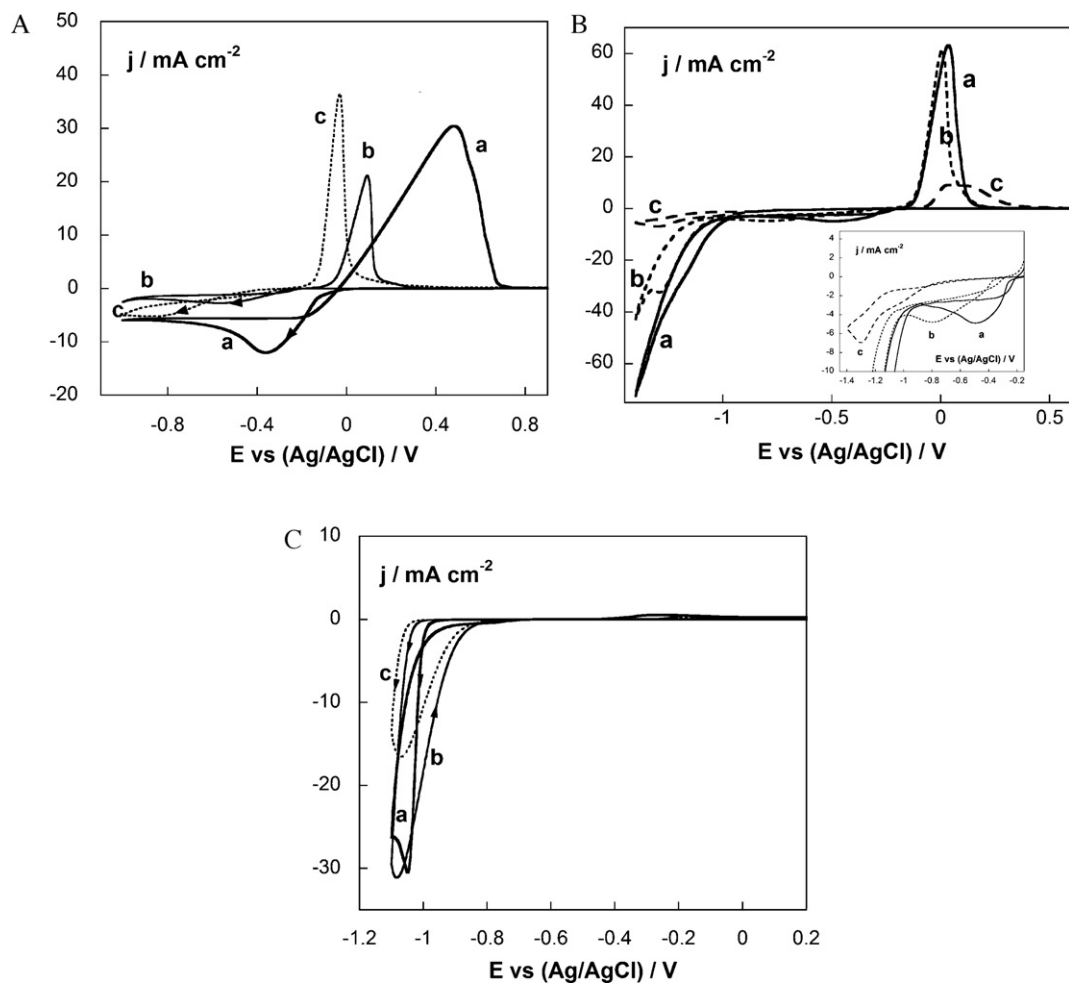


Fig. 2. Cyclic voltammograms at $\nu = 50 \text{ mV s}^{-1}$, vitreous carbon, $\omega = 0 \text{ rpm}$ for solutions: (A) at pH=4, $[\text{Cu(II)}] = 0.025 \text{ M}$ and $[\text{Na}_3\text{C}_6\text{H}_5\text{O}_7]$: (curve a) 0 M, (curve b) 0.1 M, (curve c) 0.25 M; (B) $[\text{Cu(II)}] = 0.025 \text{ M}$ and $[\text{Na}_3\text{C}_6\text{H}_5\text{O}_7] = 0.25 \text{ M}$: (curve a) pH=3, (curve b) pH=4, (curve c) pH=6; (C) at pH=4, $[\text{Ni(II)}] = 0.50 \text{ M}$ and $[\text{Na}_3\text{C}_6\text{H}_5\text{O}_7]$: (curve a) 0 M, (curve b) 0.1 M, (curve c) 0.25 M.

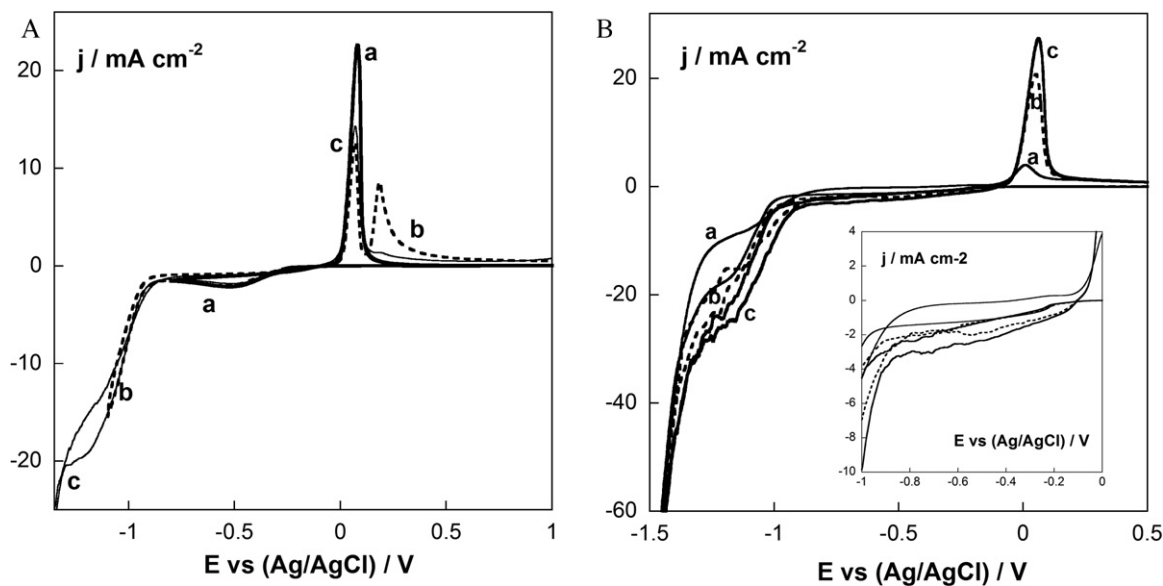


Fig. 3. Cyclic voltammograms of $0.25 \text{ M Ni(II)} + 0.0125 \text{ M Cu(II)} + 0.25 \text{ M Na}_3\text{C}_6\text{H}_5\text{O}_7$ solution, at $\nu = 50 \text{ mV s}^{-1}$, vitreous carbon. (A) pH=4, $\omega = 0 \text{ rpm}$ and different cathodic limits: (curve a) -800 , (curve b) -1100 and (curve c) -1400 mV . (B) pH=5: (curve a) $\omega = 0$, (curve b) $\omega = 300$ and (curve c) $\omega = 550 \text{ rpm}$. Inset: detail of currents.

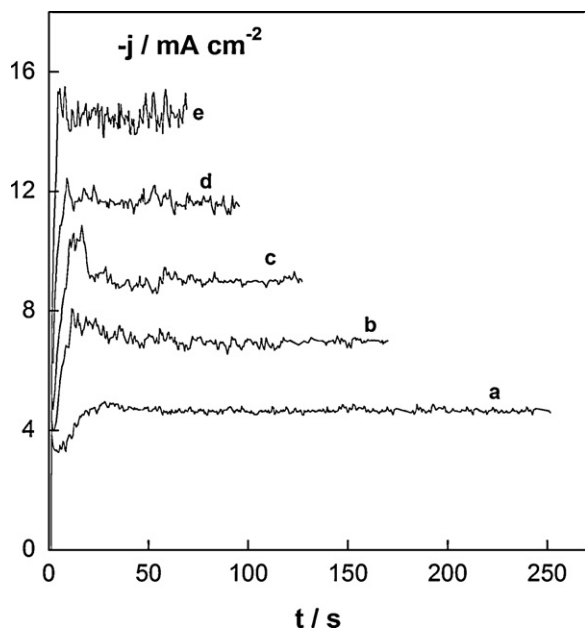


Fig. 4. Potentiostatic curves of 0.25 M Ni(II) + 0.0125 M Cu(II) + 0.25 M Na₃C₆H₅O₇ solution, pH = 5, at $\omega = 300$ rpm, vitreous carbon at different deposition potentials: (a) –980, (b) –1000, (c) –1020, (d) –1030 and (e) –1050 mV.

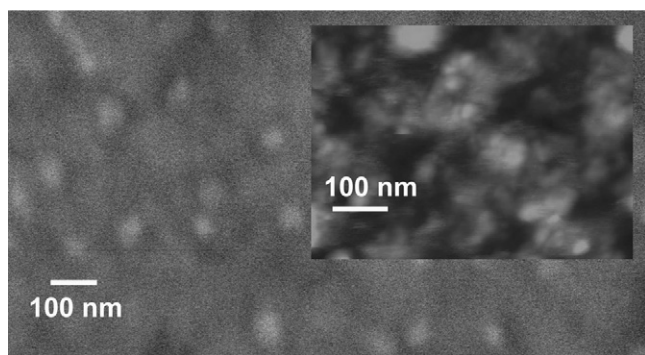


Fig. 5. SEM micrograph of a Ni–Cu deposit (28 wt.% Cu) obtained at pH = 5 from 0.25 M Ni(II) + 0.0125 M Cu(II) + 0.25 M Na₃C₆H₅O₇ solution. Inset of the figure shows an AFM detail.

selected stirring conditions lead to deposits of constant composition, a constant alloy composition throughout deposit thickness was obtained.

The crystalline structures of Ni–Cu deposits of different thickness and composition were analysed using XRD and compared with those of Ni deposits obtained from similar baths without Cu(II).

Table 1

Percentage of nickel in Ni–Cu deposits prepared potentiostatically under stirred conditions ($\omega = 300$ rpm) over vitreous carbon from the 0.25 M Ni(II) + 0.0125 M Cu(II) + 0.25 M Na₃C₆H₅O₇ solution at different pH.

pH = 4		pH = 5		pH = 6	
–E (mV)	Ni (wt.%)	–E (mV)	Ni (wt.%)	–E (mV)	Ni (wt.%)
960	12.5	950	12.4	950	16.4
980	42.2	980	43.4	960	21.9
1000	51.6	1000	53.2	970	28.7
1020	62.4	1020	64.9	990	43.4
1030	65.2	1030	68.7	1000	51.7
1040	69.2	1040	71.7	1020	67.3
1050	69.7	1050	71.9	1040	72.8
				1050	73.0

All potentials are referred to a Ag/AgCl/1 mol dm^{–3} NaCl reference electrode.

Nickel deposits were crystalline, showing a cubic face-centred (fcc) structure and 200 preferential orientation (Fig. 6). Copper incorporation into the deposit maintains the fcc phase but shifts the diffraction peaks to lower angles and induces an 111 preferred orientation (Fig. 6); the diffraction peaks appear at intermediate positions between those of pure Ni and Cu, the specific position depending on the Cu percentage in the deposits. A solid solution is always formed between both metals.

The results of this screening step indicate that the deposit composition could be modulated as a function of electrodeposition conditions. For a fixed solution, nickel percentage increases both as the applied potential was made more negative and upon increasing solution pH. However, using the selected both [Ni(II)]/[Cu(II)] ratio and citrate concentration, the expected nickel percentages are lower than the proposed as objective, even at the higher pH solution. On the other hand, in the solution of pH = 6 precipitates were observed after 15 days of preparation at difference that occurs when other salts were used to develop the electrolytic bath [37].

3.2.2. Optimization step

According to these results optimization step was made pursuing two objectives: to avoid instabilities in the solutions and to ensure greater nickel percentages. Solutions prepared at pH = 6 were discarded due to the instabilities observed in the screening step. Thus, solution pH was maintained in the $4 \leq \text{pH} \leq 5$ range. In order to prevent precipitations, the citrate concentration was reduced to 0.18 M in this optimization step. Simultaneously, to enhance the Ni percentage into the deposits, the ([Ni(II)]/[Cu(II)]) ratio was increased, as the manner that the nickel concentration was ranged between $0.30 \leq \text{Ni(II)} \leq 0.40$ M, maintaining the copper concentration. Applied potentials were selected according to the corresponding voltammetric study, and were constrain to those that led to rich nickel deposits. Samples of –50 mC on vitreous carbon were prepared. Potentiostatic curves showed the general profile obtained previously (Fig. 7). Fig. 8 shows the dependence of the nickel percentage with the potential for deposits prepared from the solutions containing 0.3 or 0.4 M of Ni(II) at pH 4.5 and 5. The increase in Ni(II) actually confirms the expected increase of nickel percentage at the more negative applied potentials, in spite of the diminution of citrate concentration. As it was observed also in the screening step, nickel content increased as solution pH increased and applied potential decreased. Stabilization of nickel percentage was attained at the more negative applied potentials, more negative values than those applied using the conditions tested in the screening step. This stabilization of nickel percentage would facilitate the preparation of constant composition layers when no flat substrates are used. Deposits prepared from the solutions tested in this step were also homogeneous, compact and showed a metallic sheen.

According to the overall results obtained, in the $4 \leq \text{pH} \leq 5$ range, solutions containing [Ni(II)]/[Cu(II)] > 20 and 0.18 M citrate concentration were useful to obtain the higher Ni percentages, maintaining the necessary quality of deposits. In order to assure stability, avoiding precipitation processes we select the solutions at pH 4.5 to test the preparation of Ni–Cu deposits. This solution pH allows a wide margin to prepare deposits of less of 100 wt.% of nickel. These solutions remained stable at least three months after preparation.

For later application on industrial substrates, these bath compositions established from the optimization step, using vitreous carbon electrode as substrate, were tested on metallic ones. Compact deposits up to dozens of microns thick were obtained on brass and inox steel. The inox steel electrode was used as test substrate for the electroforming procedure, taking advantage of its non-adherence to the deposits. The Ni–Cu deposits can be easily detached of the inox steel, which facilitated the layer

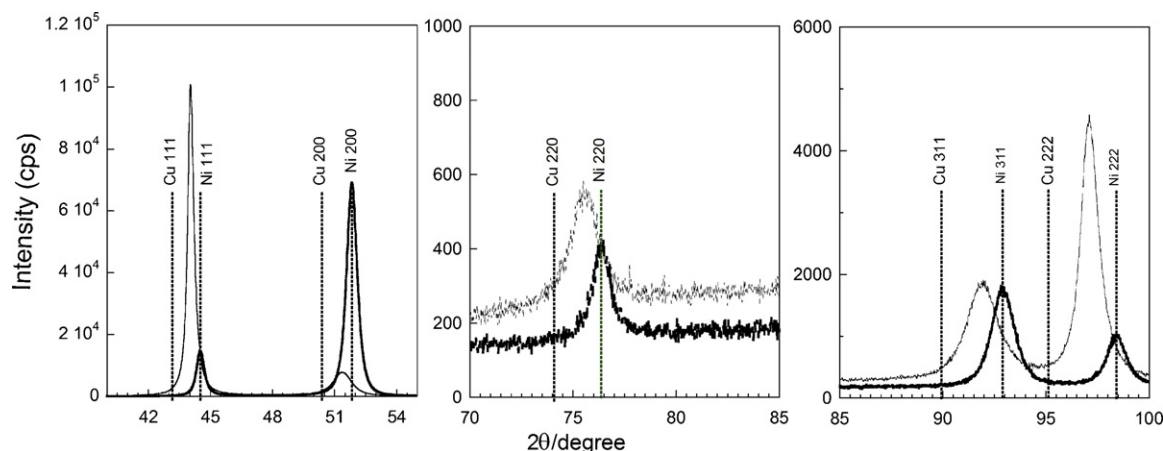


Fig. 6. Three details of the X-ray diffractograms of deposits obtained from 0.25 M Ni(II) + y M Cu(II) + 0.25 M $\text{Na}_3\text{C}_6\text{H}_5\text{O}_7$ solution (a) $y=0$, pure Ni (black line) and (b) $y=0.0125$, Ni–Cu (33 Cu wt.%) (grey line).

characterization without substrate interference. When the deposits prepared from the developed baths were detached from the inox, tensile stress was observed because they were slightly bent.

Saccharine was selected as agent to reduce the tensile stress of the deposits; its concentration was varied in the 0.3–1 g/dm³ range. Saccharine did not affect the onset of the deposition process in voltammetric experiments and no significant variation in film composition was observed with respect to the corresponding condition in a saccharine-free bath, but its presence inhibits stress, detached deposits obtained on planar substrates maintaining planarity. 0.5 g/dm³ saccharine concentration was sufficient to ensure deposit quality. The addition of saccharine did not modify solution stability, which remained also stable at least three months after preparation.

Ni–Cu deposits of variable composition were prepared on inox electrode, from solutions in which the [Ni(II)]/[Cu(II)] was moved between 24 and 32, applying different and sufficiently negative potentials. In these conditions shiny, silvery-bright and smooth Ni–Cu deposits up to 92 wt.% of Ni were obtained. Moreover, for all

Ni–Cu deposits obtained, a good current efficiency, ranged between 68 and 75%, was obtained (Fig. 9). Current efficiency (η) has been evaluated by comparing the charge involved in the deposit production (Q_{effect}), calculated from the real deposit weight, with the total charge passed (Q_{flow}) during deposition process.

$$\eta = \frac{Q_{\text{effect}}}{Q_{\text{flow}}} \times 100 \quad (1)$$

3.3. Characterization of Ni–Cu deposits obtained on inox steel

Samples of 5 cm × 2.5 cm were electrodeposited at different conditions and once prepared Ni–Cu deposits were easily detached from the substrate due to their low adherence.

3.3.1. Structural characterization

X-ray diffraction was used also to characterise the Ni–Cu deposits. Pure-nickel electrodeposits obtained in similar conditions

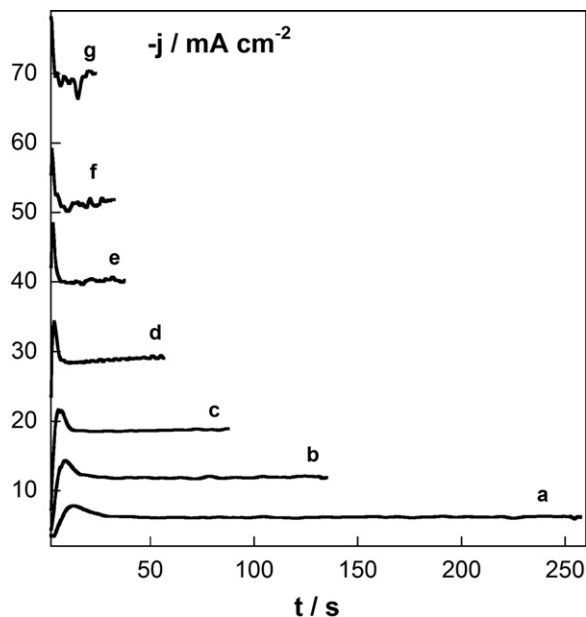


Fig. 7. Potentiostatic curves of 0.40 M Ni(II) + 0.0125 M Cu(II) + 0.18 M $\text{Na}_3\text{C}_6\text{H}_5\text{O}_7$ solution, pH = 4.5 at $\omega = 300$ rpm, vitreous carbon at different deposition potentials: (a) –950, (b) –980, (c) –1010, (d) –1040, (e) –1070, (f) –1100 and (g) –1130 mV.

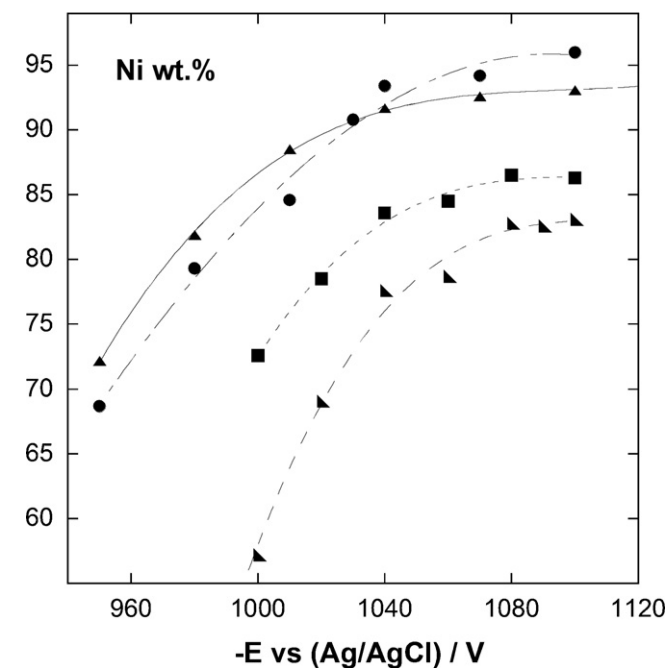


Fig. 8. Composition of deposits obtained from x M Ni(II) + 0.0125 M Cu(II) + 0.18 M $\text{Na}_3\text{C}_6\text{H}_5\text{O}_7$ solution: (\blacktriangleright) $x=0.30$, pH = 4.5, (\blacksquare) $x=0.30$, pH = 5, (\bullet) $x=0.40$, pH = 4.5, (\blacktriangle) $x=0.40$, pH = 5.

Table 2
Position of the main diffraction peaks and estimated grain size (D) for electrodeposited Ni and Ni–Cu alloys with low Cu percentage.

	111		200		311		222	
	2θ (°)	D (nm)						
Electrodeposited Ni	44.57	19	51.83	10	92.92	8	98.45	8
Ni–Cu (14 wt.% Cu)	44.34	17	51.60	9	92.52	6	97.90	8
Ni–Cu (19 wt.% Cu)	44.25	18	51.50	9	92.34	6	97.72	8

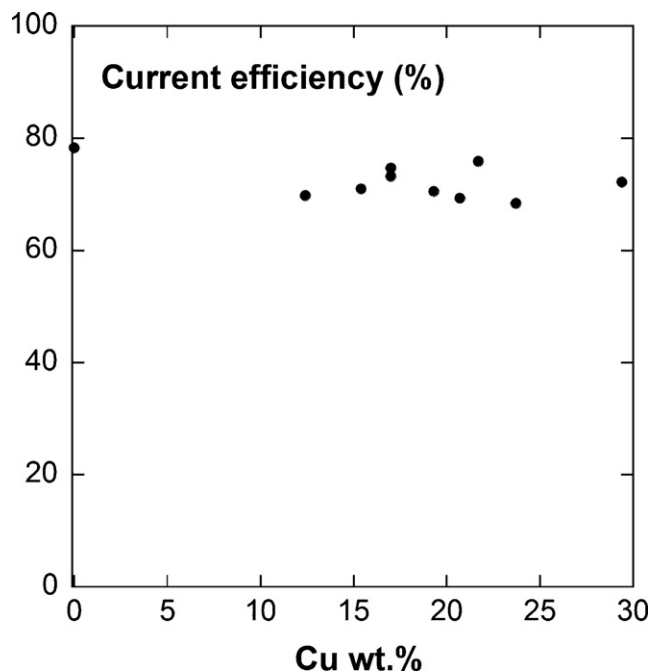


Fig. 9. Dependence of current efficiency as a function of copper content in the deposit. Deposits obtained on inox substrate at pH=4.5 from x M Ni(II) + 0.0125 M Cu(II) + 0.18 M $\text{Na}_3\text{C}_6\text{H}_5\text{O}_7$ + 0.5 g dm^{-3} saccharine, $0.3 \leq x \leq 0.4$ M solutions.

using a free-copper nickel bath were also analysed as reference. Crystalline deposits of fcc structure were obtained as over vitreous carbon electrode. Their grain size (D) was estimated from the Debye–Sherrer analysis of the main diffraction peaks [43]. Table 2 shows the values obtained from some representative samples. Ni and Ni–Cu prepared deposits were nanocrystalline, showing a certain crystalline anisotropy. Values of D in the 8–19 nm range were obtained. No significant variation in the grain size was observed

when moderate percentages of copper were included in the Ni fcc lattice.

3.3.2. Mechanical characterization

Measurements of both HV hardness and Young's modulus of some of the films prepared revealed that the incorporation of copper in nickel deposits does not cause any significant variation in mechanical properties. HV hardness values (Fig. 10A) were higher than those corresponding to the electrodeposited nickel (HV=670 MPa) obtained from a similar bath containing only the single metal. All them were higher than that of annealed polycrystalline bulk Ni (HV=638 MPa). The high hardness values can be attributed to the fine grain size that has been obtained by electrodeposition of these series of Ni–Cu alloys. Composition may have effects on the hardness, but predominantly, a very small grain size can increase the polycrystalline film hardness as compared to that of the micron-sized polycrystalline bulk material. The increase in hardness gives consistency to the film, always beneficial in coating applications. The deposits prepared showed similar values of the Young's modulus to those of electrodeposited Ni (67 GPa) (Fig. 10B) demonstrating that alloying Ni with moderate percentages of Cu does not cause notable changes in material elasticity.

3.3.3. Electrical characterization

Coatings to be used in astronomy instruments may be valuable if they have a good electrical conductivity. Fig. 11 shows the resistivity of different Ni–Cu alloys and pure Ni deposits. The resistivity of the electrodeposited nickel (90 $\text{n}\Omega\text{ m}$) appears to be somewhat higher than the standard resistivity of bulk nickel (72.5 $\text{n}\Omega\text{ m}$). This bulk value is given for well-annealed Ni with micron-sized grains [44]. Higher electrical resistivity of electrodeposited Ni with respect to the bulk Ni value has been reported, and found to be dependent of the preparation method [45], more precisely; it has been attributed to the nanocrystalline grain size of the electrodeposited Ni [46]. The incorporation of copper atoms in our materials causes a resistivity increase of the foil samples. Resistivity increases linearly with Cu content within the range examined (up to 29 wt.%

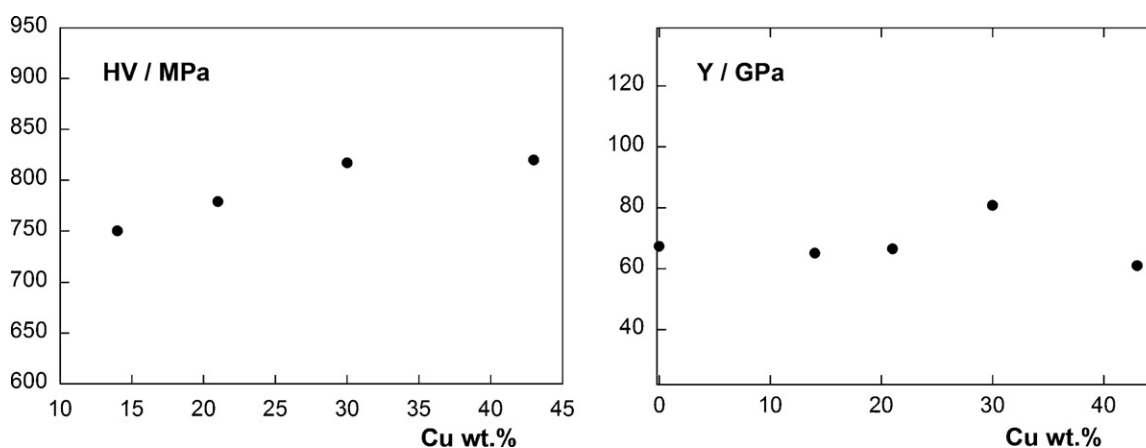


Fig. 10. Dependence of (A) microhardness and (B) Young modulus for Ni–Cu deposits as a function of copper content. Deposits obtained on inox substrate at pH=4.5 from x M Ni(II) + 0.0125 M Cu(II) + 0.18 M $\text{Na}_3\text{C}_6\text{H}_5\text{O}_7$ + 0.5 g dm^{-3} saccharine, $0.3 \leq x \leq 0.35$ M solutions.

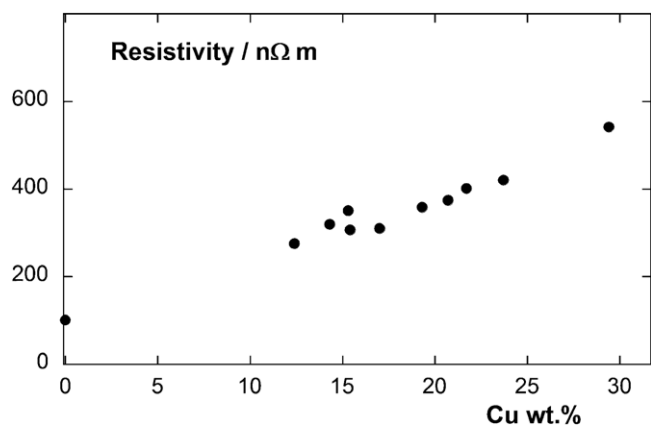


Fig. 11. Dependence of electrical resistivity of Ni–Cu deposits as a function of copper content, measured by four electrical contacts with van der Paw geometry. Deposits obtained on inox substrate at pH = 4.5 from x M Ni(II) + 0.0125 M Cu(II) + 0.18 M $\text{Na}_3\text{C}_6\text{H}_5\text{O}_7$ + 0.5 g dm^{-3} saccharine, $0.3 \leq x \leq 0.4$ M solutions.

copper). Other samples, with very high Cu, content showed low electrical resistivity values. This experimental behaviour was to be expected: alloy resistivities are always higher than the resistivities of the pure metals. The incorporation of a different element in the crystalline network of a pure metal hinders the electron mobility and consequently the electrical resistance increases. All the different commercial nickel alloys show an electrical resistivity higher than that of pure nickel. For the electrodeposited alloys, the small crystalline grain size of the deposited materials may additionally contribute to increase their resistivity [46].

3.3.4. Optical characterization

Visually, the deposits were silvery-bright. The presence of copper (<30 wt.%) did not modify qualitatively the colour or the brightness aspect of the material. The gloss measurements of deposits were carried out. Fig. 12 shows that by increasing copper percentage, gloss decreased smoothly. These low differences in brightness can be explained taking into account the preparation method. Whatever was the solution used, samples with low copper percentages were obtained by applying the more negative potentials, consequently nucleation is favoured, grain size is diminished and light reflection is enhanced. Nevertheless, the

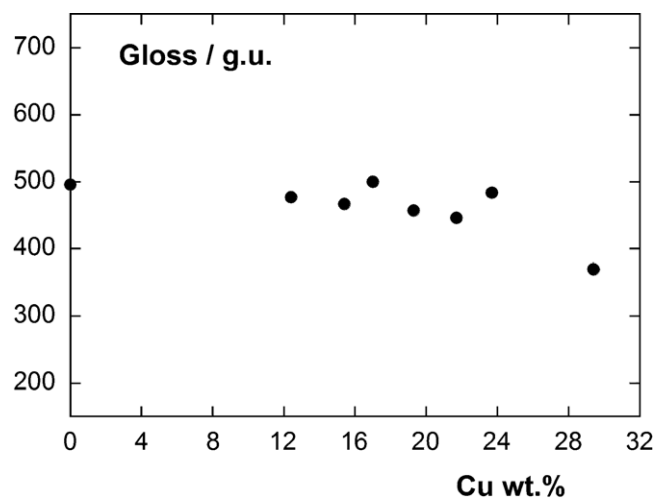


Fig. 12. Dependence of gloss (in gloss units) of electrodeposited Ni–Cu with copper percentage. Deposits obtained on inox substrate at pH = 4.5 from x M Ni(II) + 0.0125 M Cu(II) + 0.18 M $\text{Na}_3\text{C}_6\text{H}_5\text{O}_7$ + 0.5 g dm^{-3} saccharine, $0.3 \leq x \leq 0.4$ M solutions.

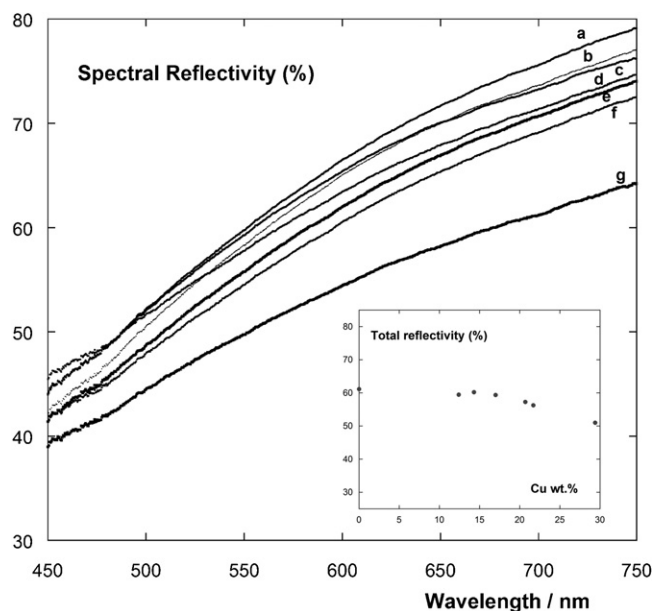


Fig. 13. Spectral reflectivity of the pure Ni sample (curve a) and the Ni–Cu alloys (curve b) 12.4, (curve c) 14.3, (curve d) 17, (curve e) 20.7, (curve f) 21.7 and (curve g) 29.4 Cu wt.% measured in the visible range. *Inset:* Total reflectivity of the Ni and Ni–Cu alloy samples as calculated from the integration of the spectral reflectivity data in the range 400–750 nm. Deposits obtained on inox substrate at pH = 4.5 from x M Ni(II) + 0.0125 M Cu(II) + 0.18 M $\text{Na}_3\text{C}_6\text{H}_5\text{O}_7$ + 0.5 g dm^{-3} saccharine solution, $0.3 \leq x \leq 0.4$ M solutions.

surface roughness was low (profile parameters with 50–80 nm values for rms and 40–62 nm for Ra were obtained).

Spectral reflectivity measurements, between 450 nm and 750 nm, confirmed that the colour of nickel was not changed significantly by copper alloying. Pure Ni electrodeposit showed (Fig. 13, curve a) a spectral reflectivity that is in close agreement with that of polished nickel metal samples [47]. The reflectivity curves for the Ni–Cu samples (Fig. 13, curve b–g) showed a very similar shape to that obtained for pure nickel sample and slightly lower reflectivity, except for that with 29.4 wt.% Cu for which the loss was significant. Similar shape means that the hue of these samples is very similar to that of the pure Ni. The spectral reflectivity decrease was less pronounced for the short wavelength colours, meaning a slight shift from yellowish to bluish hue, but this was not appreciable by visual observation. From the reflectivity spectra of each sample, we can calculate a “total reflectivity” in the visible range by integrating the spectra over the 450–750 nm range, and normalise the result to the same result calculated for the 100% reflectivity flat spectrum obtained with the standard reference samples. This integrated reflectivity (inset in Fig. 13) has been closely compared to the relative gloss values measured with white light with the glossmeter. A good concordance between both kinds of measures was observed, as it expected.

4. Conclusions

Useful formulations leading electrochemically produced Ni–Cu deposits with good gloss, reflectivity, mechanical properties and which could be implemented in an electroforming process have been developed.

For each separate metal, the study of the influence of both citrate concentration and pH solution put the bases for the design of a first general formulation ([Ni(II)] = 0.25 M, [Cu(II)] = 0.0125 M, [citrate] = 0.25 M). An initial study over vitreous carbon electrode and different pH values has permitted us to select the codeposition potential range for each formulation tested and to establish the pH

and applied potential effect in the electrodeposition processes and to prepare Ni-rich Ni–Cu deposits. Solid solution formation occurs, which allows one modulating the composition of the deposit as a function of both bath composition and electrodeposition conditions.

In a subsequent step, a simple factorial analysis was used to optimise the bath. Because of the instabilities observed at pH 6 in the screening step, the analysis was restricted to pH values in the 4–5 range and, in view of the not high enough nickel percentages attained, the nickel (II) concentration was raised. The results obtained over vitreous carbon electrode were extended to metallic substrates in order to check for electroforming possibilities. Finally, stable solutions with $[\text{Cu(II)}] = 0.0125 \text{ M}$ [sodium citrate] = 0.18 M, $[\text{Ni(II)}]$ in the 0.3–0.4 M range and $[\text{saccharin}] = 0.5 \text{ g/dm}^3$ led to deposits with 10–30 wt.% of Cu and low stress over an inox steel flat substrate. For each solution, there is a potential range at sufficient negative potential values in which the Ni–Cu composition remains almost constant. This could facilitate the maintenance of a constant composition during the plating over a non-planar substrate. Since at these conditions the composition was only slightly dependent on the applied potential, constant composition of the deposits is expected for samples with no flat geometrical shapes.

The optical, mechanical and electrical properties of the optimised Ni–Cu deposits make them an alternative to pure nickel for reflective applications. Ni–Cu alloy with 10 wt.% Cu shows reflectivity similar to that of pure electrodeposited Ni and Ni–Cu with 20 wt.% of Cu shows only a slight decrease. Moreover, the mechanical properties of these alloys improve with respect to those of the corresponding nickel coating.

Nevertheless, the high $[\text{Ni(II)}]/[\text{Cu(II)}]$ ratios supposes a periodic control of the solution to replenish the consumed copper (II), but this is easily attainable in view of the large number of analysis methods available for these electroactive metals.

Acknowledgements

This paper was supported by contract CTQ2010-20726 and contract FUNCOAT CSD2008-0023, from the Ministerio de Ciencia e Innovación (MICINN) and the FEDER fund. This work has also financial assistance from the Bilateral Project between Politecnico di Milano (Italy) and Universitat de Barcelona (Spain) (HI2008-0058). The authors wish to thank the Centres Científics i Tecnològics – CCI TUB (UB) for the use of this equipment.

References

- [1] W.J. Egle, H. Bulla, P. Kaufmann, B. Aschenbach, H.W. Braeuninger, *Opt. Eng.* 29 (10) (1990) 1267.
- [2] R. Hudec, L. Pina, L. Sveda, A. Inneman, V. Semencova, V. Brozek, M. Mika, M. Skulinova, R. Kacerovsky, J. Sik, A. Zentko, in: A. Wilson (Ed.), *Proceedings of X-ray Universe 2005 (ESA SP-604)*, El Escorial, Madrid, 2005, p. 969.
- [3] S. Romaine, S. Basso, R.J. Bruni, W. Burkert, O. Citterio, V. Cotroneo, D. Engelhaupt, M. Freyberg, J. Gorenstein, P. Gubarev, G. Hartner, F. Mazzoleni, S. O'Dell, G. Pareschi, B.R. Ramsey, C. Speegle, D. Spiga, Development of a prototype nickel optic for the Constellation-X hard X-ray telescope, in: S.L. O'Dell, G. Pareschi (Eds.), *Proceedings of SPIE: Optics for EUV, X-ray and gamma-ray*, vol. 6688, 29–30 August, San Diego, CA, 2007, p. 668804, doi:10.1117/12.736063.
- [4] R. Banham, G. Valsecchi, A. Valenzuela, Precision Replication by nickel electroforming, in: *ASPE Proceedings. ASPE Precision Fabrication and Replication*, October 31–November 5, Monterey, CA, 1999.
- [5] H.-M. Zhang, Y.-G. Guo, L.-J. Wan, C.-L. Bai, *Chem. Commun.* 1 (24) (2003) 3022.
- [6] M. Jafarian, F. Forouzandeh, I. Danaee, F. Gopal, M.G. Mahjani, *J. Sol. State Electrochem.* 13 (8) (2009) 1171.
- [7] J.L. Pinilla, I. Suelves, M.J. Lázaro, R. Moliner, J.M. Palacios, *Int. J. Hyd. Energy* 35 (18) (2010) 9801.
- [8] G. Xiao, C.L. Chien, *J. Appl. Phys.* 61 (1987) 4061.
- [9] J. Toth, L.F. Kiss, E. Toth-Kadar, A. Dinia, V. Pierron-Bohnes, I. Bakonyi, *J. Magn. Magn. Mater.* 198–199 (1999) 243.
- [10] E. Toth-Kadar, L. Peter, T. Becsei, J. Toth, L. Pogany, T. Tarnoczi, P. Kamasa, I. Bakonyi, G. Lang, A. Cziraki, W. Schwarzacher, *J. Electrochem. Soc.* 147 (2000) 3311.
- [11] I. Kazeminezhad, W. Schwarzacher, *J. Solid State Electrochem.* 8 (2004) 187.
- [12] M. Alper, M.C. Baykul, L. Peter, J. Toth, I. Bakonyi, *J. Appl. Electrochem.* 34 (2004) 841.
- [13] D. Bazavan, R. Bazavan, I. Enculescu, E. Matei, C. Necula, L. Ion, S. Antohe, *Optoelectron. Adv. Mater. Rapid Commun.* 3 (5) (2009) 484.
- [14] W.A. Badawy, K.M. Ismail, A.M. Fathi, *J. Appl. Electrochem.* 35 (2005) 879.
- [15] R.G. Delatorre, M.L. Sartorelli, A.Q. Schervenski, A.A. Pasa, S. Güths, *J. Appl. Phys.* 93 (2003) 6154.
- [16] S. Serrano-Guisan, L. Gravier, M. Abid, J.-Ph. Ansermet, *J. Appl. Phys.* 99 (8, Pt. 3) (2006), 08T108/1.
- [17] W. Glatz, E. Schwyter, L. Durrer, Ch. Hierold, *J. Microelectromech. Syst.* 18 (3) (2009) 763.
- [18] I. Mizushima, M. Chikazawa, T. Watanabe, *J. Electrochem. Soc.* 143 (1996) 1978.
- [19] E. Pellicer, A. Varea, S. Pané, K.M. Sivaraman, B.J. Nelson, S. Suriñach, M.D. Baró, *J. Surf. Coat. Technol.* 205 (2011) 5285.
- [20] S.K. Ghosh, G.K. Dey, R.O. Dusane, A.K. Grover, *J. Alloys Compd.* 426 (2006) 235.
- [21] I.Z. Shehata, O.S. Ayob, E.A. Bull, *Electrochemistry* 22 (3) (2006) 103.
- [22] N. Rajasekan, S. Mohan, *Trans. Inst. Met. Finish.* 89 (2) (2011) 83.
- [23] M. Ishikawa, H. Enomoto, M. matsuoaka, C. Iwakura, *Electrochim. Acta* 40 (11) (1995) 1663.
- [24] M. Zhou, N. Myung, X. Chen, K. Rajeshwar, *J. Electroanal. Chem.* 398 (1995) 5.
- [25] P. Bradley, S. Roy, D. Landolt, *J. Chem. Soc. Faraday Trans.* 92 (20) (1996) 4015.
- [26] J.R. Roos, J.P. Celis, C. Buelens, D. Goris, *Proc. Metall.* 3 (1984) 177.
- [27] K. Vu Quang, E. Chassaing, B. Le Viet, J.P. Celis, *J.R. Roos, Met. Finish.* 10 (1985) 25.
- [28] R.Y. Ying, *J. Electrochem. Soc.* 135 (1988) 2957.
- [29] E.J. Podlaha, Ch. Bonhote, D. Landolt, *Electrochim. Acta* 39 (1994) 2649.
- [30] C. Bonhote, D. Landolt, *Electrochim. Acta* 42 (15) (1997) 2407.
- [31] H. Natter, M. Schmelzer, R. Hempelmann, *J. Mater. Res.* 13 (1998) 1186.
- [32] S.K. Ghosh, A.K. Grover, G.K. Dey, M.K. Totlani, *Surf. Coat. Technol.* 126 (2000) 48.
- [33] I. Tabkovic, S. Riemer, S. Ming, A.V. Vladyslav, M. Kief, *J. Electrochem. Soc.* 152 (2005) C851.
- [34] A.R. Despic, V.D. Jovic, S. Spaic, *J. Electrochem. Soc.* 136 (1989) 6.
- [35] M. Pushpavam, K. Balakvushuan, *J. Appl. Electrochem.* 26 (1996) 1065.
- [36] E. Beltowska-Lehman, P. Ozga, *Electrochim. Acta* 43 (5–6) (1998) 617.
- [37] T.A. Green, A.E. Russell, S. Roy, *J. Electrochem. Soc.* 145 (1998) 875.
- [38] P.W. Araujo, R.G. Brereton, *Trend. Anal. Chem.* 15 (1996) 26.
- [39] L.J. Van der Pauw, *Philips Res. Rep.* 13 (1958) 1.
- [40] MEDUSA-Chemical Diagrams (2.0) and HYDRA-Hydrochemical Database (2.0) Softwares of I. Puigdomenech. <http://www.kemi.kth.se/medusa/>.
- [41] Stability constants of metal-ion complexes, in: D. Douglas, Perrin (Eds.), *Section B: Organic Ligands. IUPAC. Chemical Data Series 22*, Pergamon Press, Exeter, 1983.
- [42] B.H. Priscott, *Trans. Inst. Met. Finish.* 36 (1959) 1958.
- [43] B.D. Cullity, Debye–Sherrer equation, in: *Elements of X-ray Diffraction*, Addison Wesley, Reading, MA, 1978, 283 p.
- [44] M.J. Laubitz, T. Matsumura, P.J. Kelly, *Can. J. Phys.* 54 (1976) 92.
- [45] *ASM Metals Handbook*, vol. 2, ASM International, 10th edition, OH, 1990.
- [46] A. Cziraki, B. Fogarassy, I. Gerocs, E. Toth-Kadar, I. Bakonyi, *J. Mater. Sci.* 29 (1994) 4771.
- [47] D.J. Arrowsmith, *Gold Bull.* 19 (4) (1986) 117.